Supporting Information

Near-infrared-excited upconversion photodynamic therapy of extensively drug-resistant *Acinetobacter baumannii* based on lanthanide nanoparticles

Wenzhen Liu,[ae] Yuxiang Zhang,[ae] Wenwu You,[a] Jianqiang Su,[c] Shaohua Yu,[ae] Tao Dai,[ae] Yunmei Huang[d], Xueyuan Chen,[ae] Xiaorong Song,*[b] and Zhuo Chen*[ae]

[a] State Key Laboratory of Structural Chemistry, CAS Key Laboratory of Design and Assembly of Functional Nanostructures, and Fujian Key Laboratory of Nanomaterials, Fujian Institute of Research on the Structure of Matter, Chinese Academy of Sciences, Fuzhou, Fujian 350002, China.

[b] Institute of Environmental Analysis and Monitoring, MOE Key Laboratory for Analytical Science of Food Safety and Biology, College of Chemistry, Fuzhou University, Fuzhou, Fujian 350116, China.

[c] Key Lab of Urban Environment and Health, Institute of Urban Environment, Chinese Academy of Sciences, Xiamen, Fujian 361021, China.

[d] Academy of Integrative Medicine, Fujian University of Traditional Chinese Medicine, Fuzhou, Fujian 350122, China.

[e] University of Chinese Academy of Sciences, Beijing 100049, China.

E-mail: zchen@fjirsm.ac.cn or xrsong@fzu.edu.cn; Fax: + 86 591 63179421; Tel: +86 591 63173094

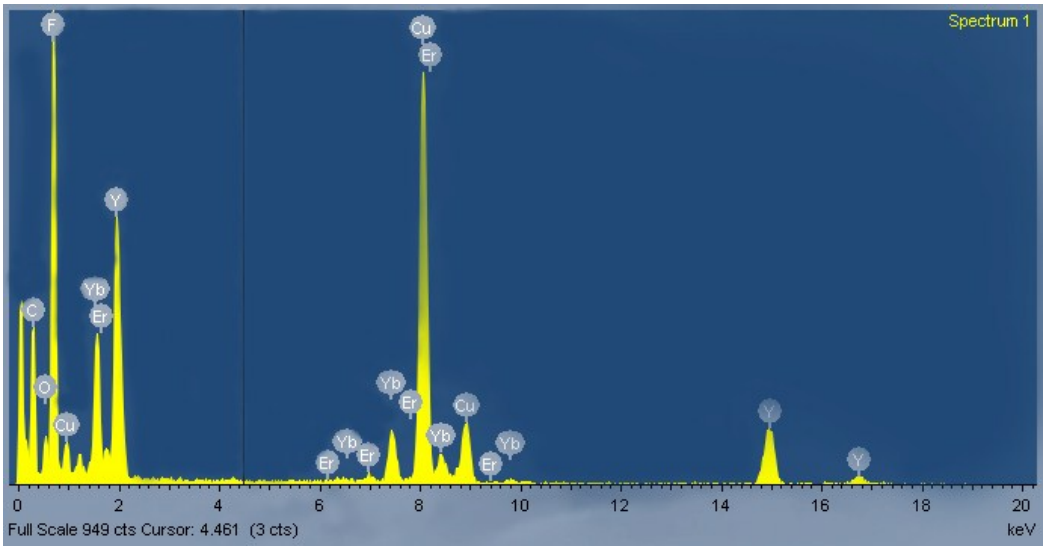

Figure S1. Energy dispersive X-ray (EDX) spectrum of $LiYF_4$:Yb/Er UCNPs. These peaks revealed the existence of Y, F, Yb and Er elements in $LiYF_4$:Yb/Er UCNPs.

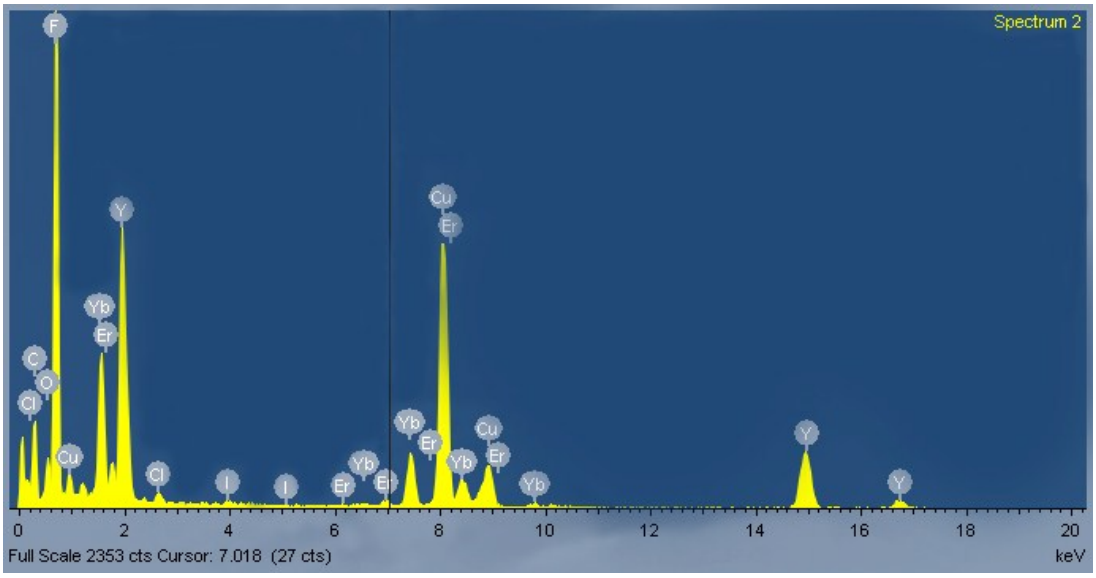

Figure S2. EDX spectrum of UCNPs-PVP-RB. The existence of Cl and I elements of RB revealed the successful loading of RB on UCNPs-PVP.

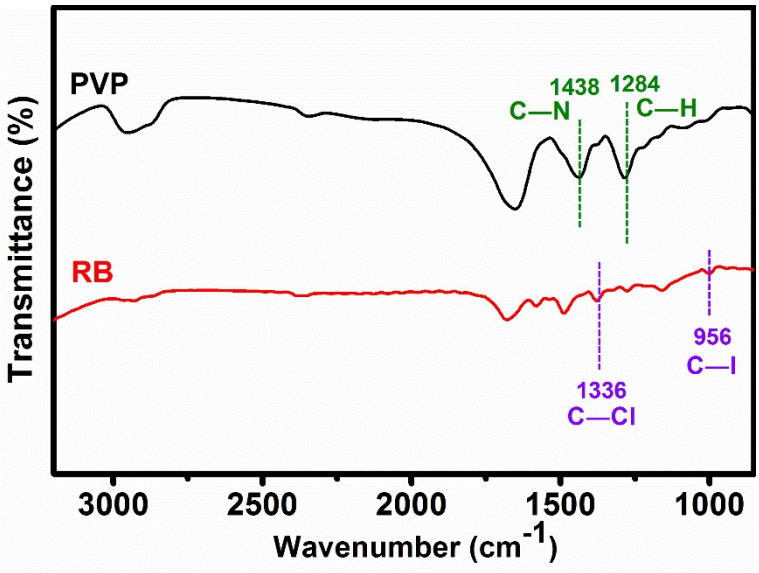

Figure S3. Fourier transform infrared (FTIR) spectra of PVP and RB. Some feature peaks and the corresponding functional groups are marked.

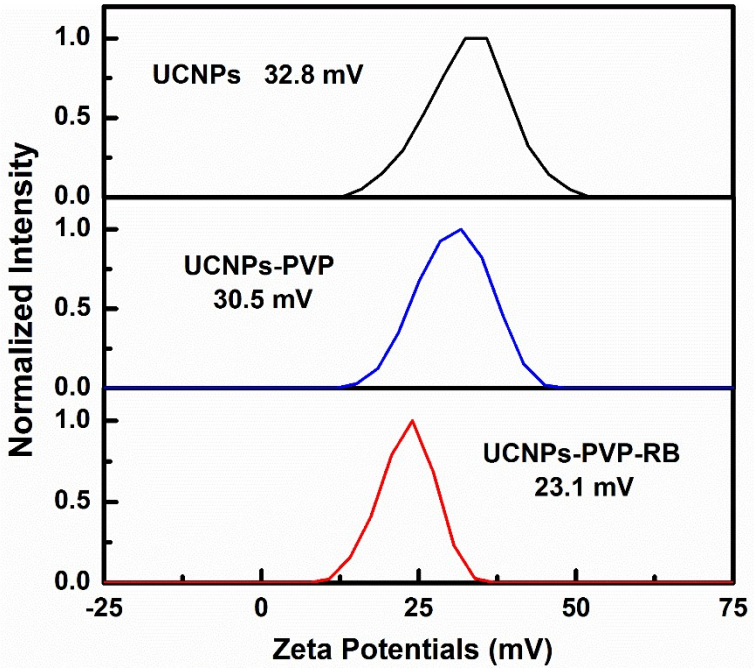

Figure S4. ζ-potentials of the UCNPs, UCNPs-PVP and UCNPs-PVP-RB obtained from dynamic light scattering measurement. The ζ-potential of the UCNPs was slightly decreased after surface coating with PVP. After loading RB, the ζ-potential of UCNPs-PVP changed from +30.5 mV to +23.1 mV.

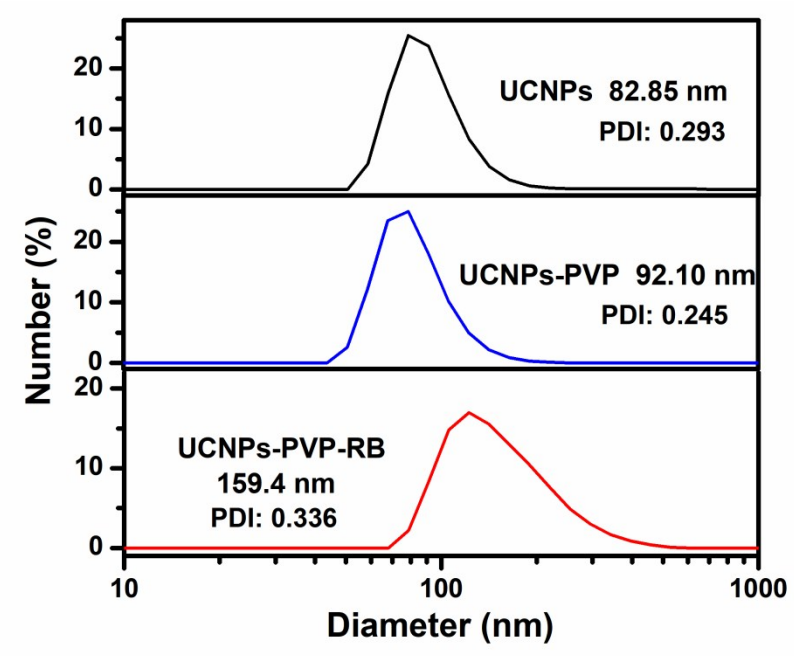

Figure S5. Hydrodynamic diameter distributions of UCNPs, UCNPs-PVP and UCNPs-PVP-RB in aqueous solutions. The mean diameters are marked.

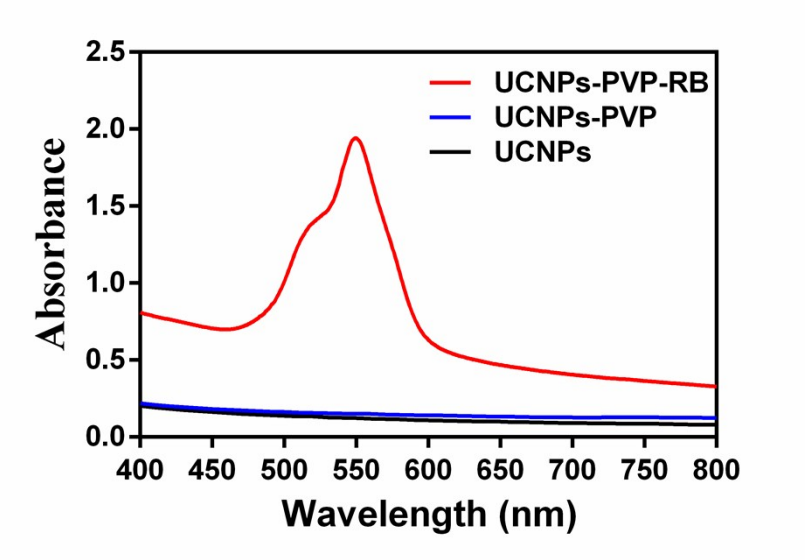

Figure S6. Absorbance spectra of UCNPs, UCNPs-PVP and UCNPs-PVP-RB in aqueous solutions. A characteristic absorption peak of RB centered at about 550 nm was observed in the UCNPs-PVP-RB, confirming the successful loading of RB on UCNPs-PVP.

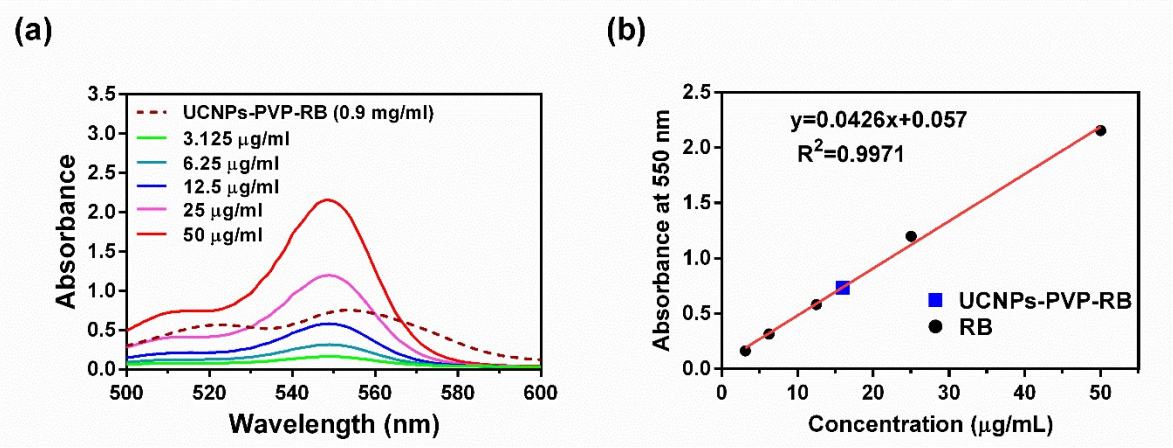

Figure S7. Quantitative analysis of RB loaded on the surface of UCNPs-PVP. (a) Absorption spectra of RB at various concentrations (3.125, 6.25, 12.5, 25 and 50 μg/mL, respectively) and the UCNPs-PVP-RB (0.9 mg/mL) in deionized water. (b) Standard curve of RB absorption in deionized water. The loading capacity of RB was about 1.8% (w/w) in UCNPs-PVP-RB.

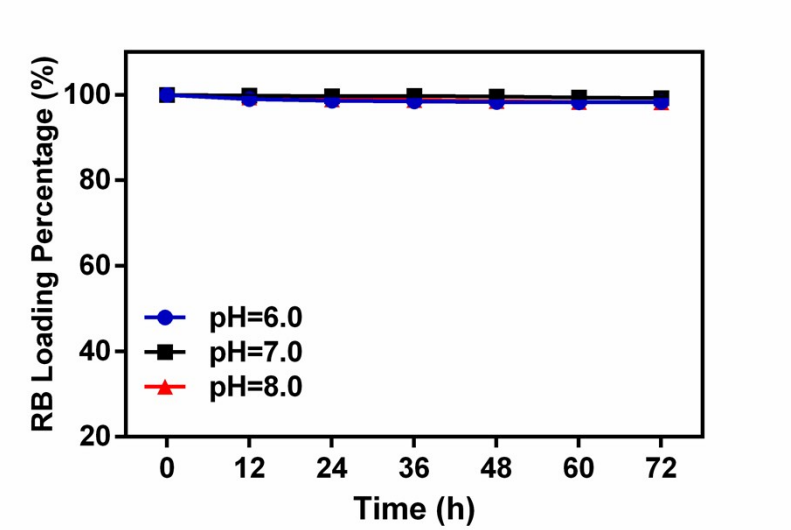

Figure S8. RB release from UCNPs-PVP-RB in saline solution at different pH values (6.0, 7.0 and 8.0). No significant release of RB in UCNPs-PVP-RB was observed during 3 days, indicating the excellent RB loading stability

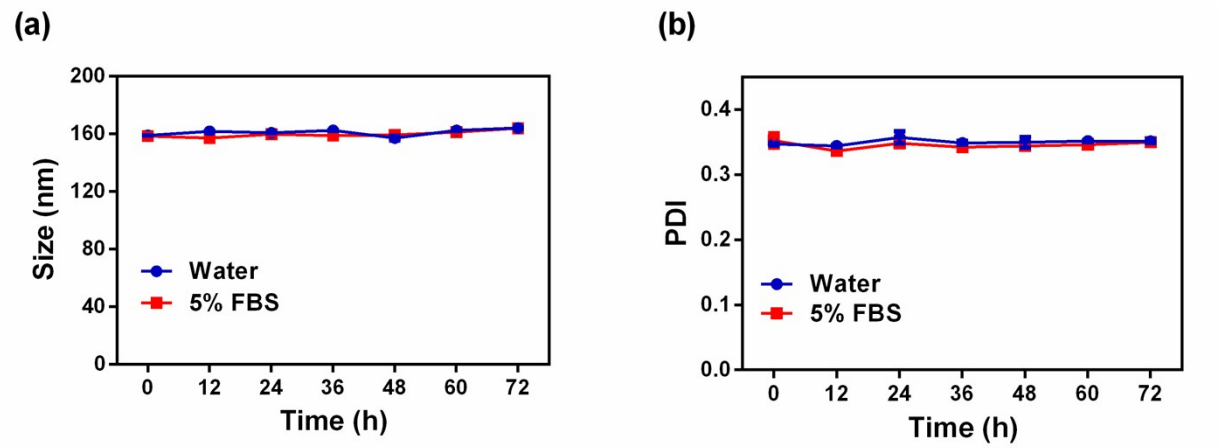

Figure S9. (a) Hydrodynamic size and (b) Polydispersity index (PDI) changes of UCNPs-PVP-RB dispersed in water and PBS containing 5% FBS for 3 days. Negligible particle aggregation was observed within 3 days, indicating the excellent colloidal stability of the nanoagents.

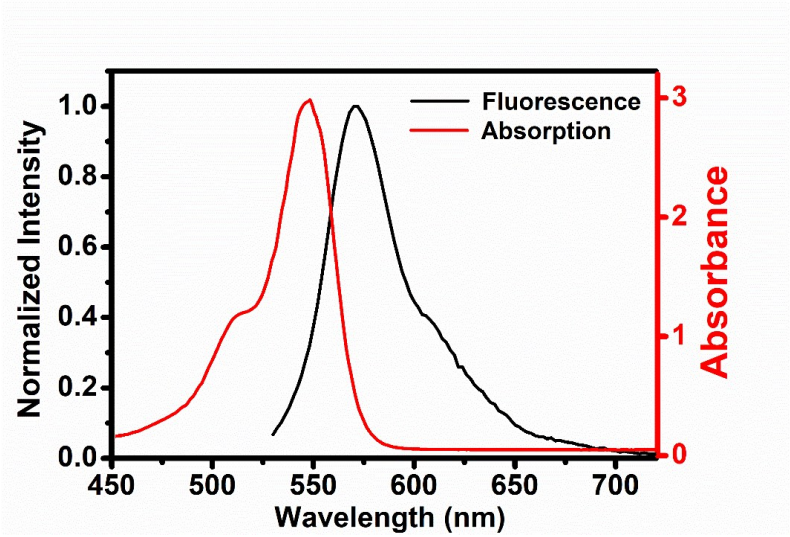

Figure S10. Absorption and emission spectra of RB in the aqueous solutions. RB showed the absorption and emission peaks at about 550 nm and 570 nm, respectively. The fluorescence was acquired with excitation of 520 nm.

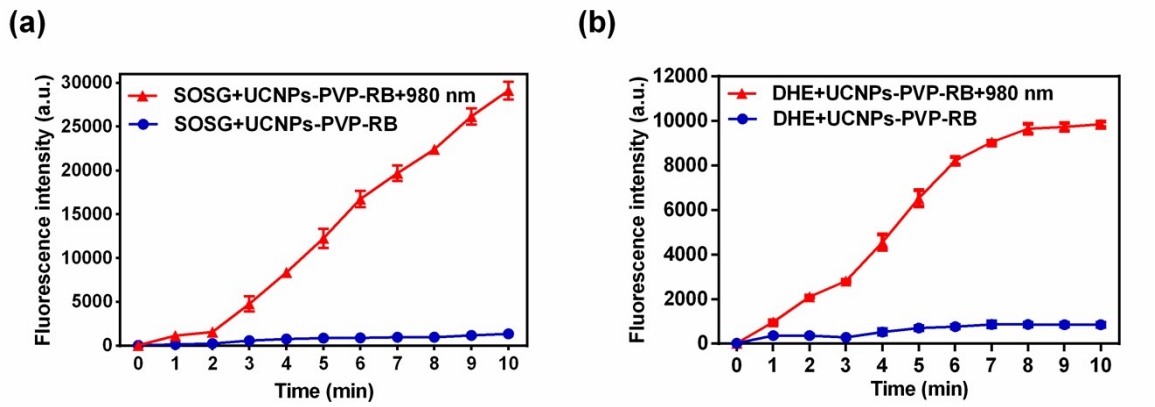

Figure S11. Analysis of generated (a) singlet oxygen and (b) superoxide ion upon irradiating UCNPs-PVP-RB solution with 980 nm laser (1 mg/mL, 1 W/cm²) by using SOSG and DHE as specific probes. The results showed the generation of both singlet oxygen and superoxide ion in UCNPs-PVP-RB.

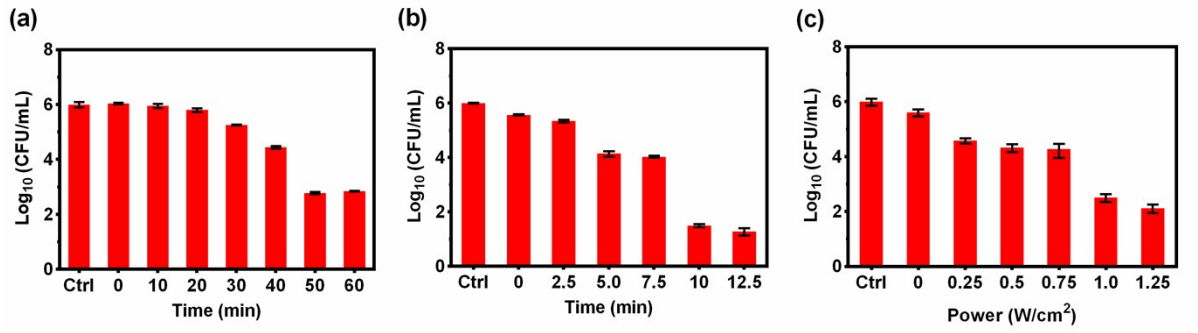

Figure S12. Viability of XDR-AB under treatments of (a) different incubation time, (b) different NIR irradiation time, and (c) different NIR laser power density. The incubation time of UCNPs-PVP-RB and XDR-AB was optimized to be 50 min. The NIR irradiation time and laser power density were optimized to be 10 min and 1 W/cm^2, respectively.

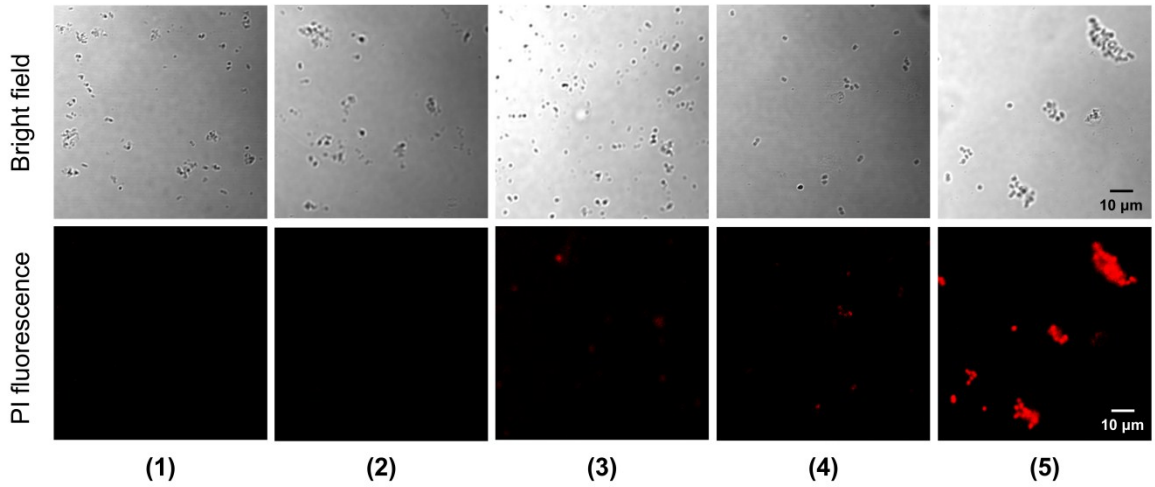

Figure S13. CLSM images of PI stained XDR-AB after different treatments. (1) 0.9% saline solution, (2) 10-min NIR irradiation (at a power density of 1 W/cm²), (3) UCNPs-PVP-RB (50 μg/mL), (4) UCNPs-PVP-RB plus 10-min NIR irradiation but without PI staining, and (5) UCNPs-PVP-RB plus 10-min NIR irradiation. Dead cells were identified by the red fluorescence of PI staining. These results demonstrated the killing effect of aPDT with UCNPs-PVP-RB triggered by NIR on XDR-AB.

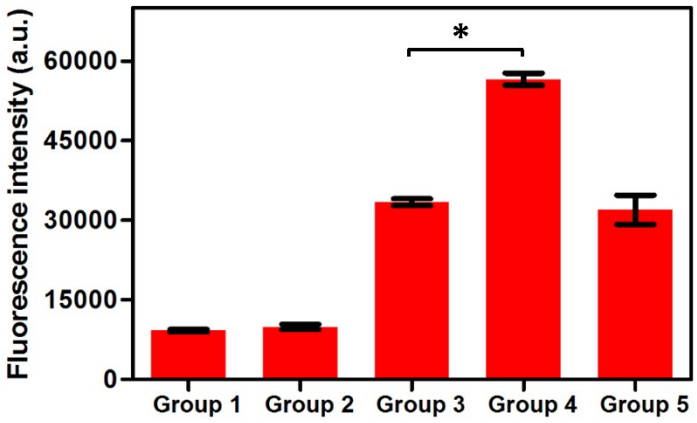

Figure S14. Fluorescence intensity of XDR-AB after different treatments and PI staining. Group 1. 0.9% saline solution. Group 2. 10-min NIR irradiation (at a power density of 1 W/cm²). Group 3. UCNPs-PVP-RB (50 μg/mL). Group 4. UCNPs-PVP-RB plus 10-min NIR irradiation. Group 5. UCNPs-PVP-RB plus 10-min NIR irradiation without bacteria. The marked "*" indicates a significant difference ($P < 0.01$) from the corresponding control group.

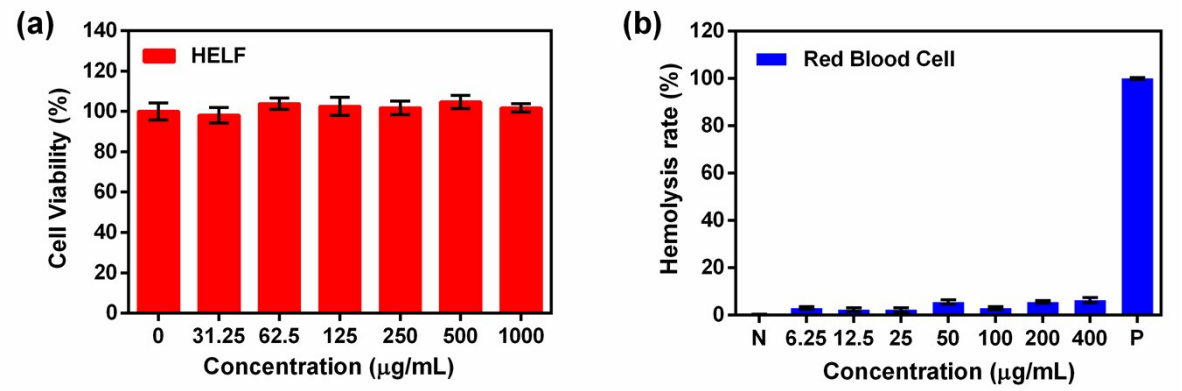

Figure S15. Biosafety of UCNPs-PVP-RB. (a) Cell viability of HELF after a 24-h incubation with various concentrations of UCNPs-PVP-RB. (b) Hemolysis assay of RBC treated with water, 0.9% saline solution, and different concentrations of UCNPs-PVP-RB. These results revealed a good biocompatibility of UCNPs-PVP-RB.

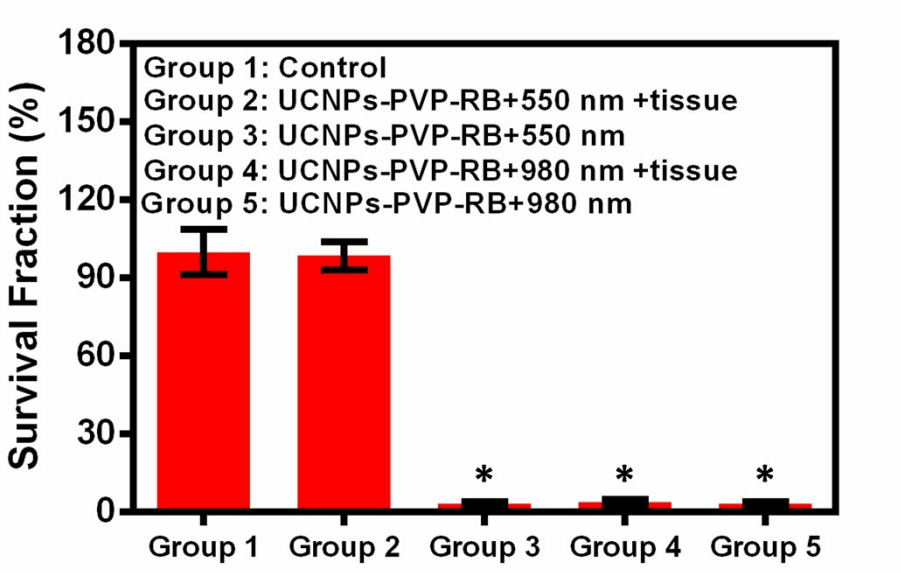

Figure S16. Survival fraction of *in vivo* XDR-AB upon various treatments. *P<0.01.

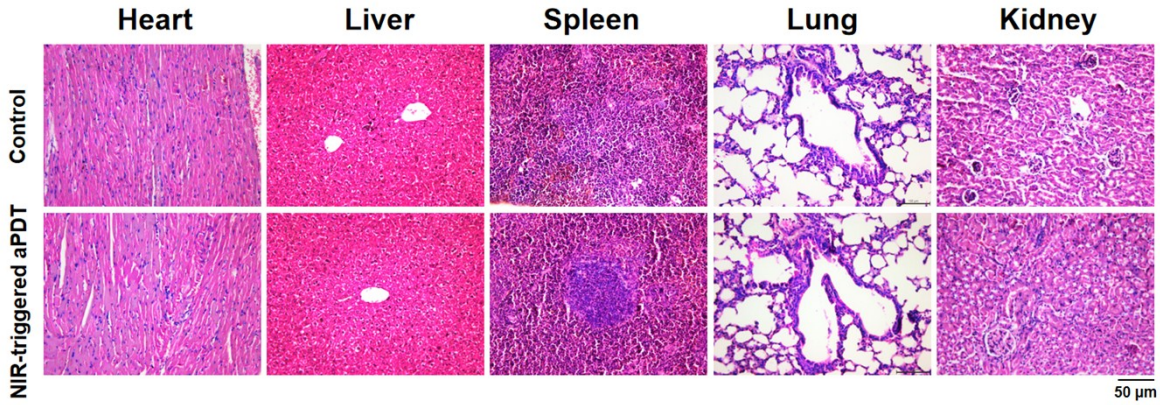

Figure S17. Representative H&E stained images of major organs from the mice of control and NIR-triggered aPDT treated groups after the therapeutic study. The results revealed no evident histopathological abnormalities or lesions in organs.